electronics

MDPI

Article

Enhancement of Signal Amplitude of Magnetostrictive-Based EMAT with Terfenol-D Coating for Stainless-Steel Specimens

Bao Liang [1], Lei Kang [2,*] and Wang Liu [1]

[1] School of Electrical and Information Engineering, Jiangsu University of Technology, Changzhou 213001, China; liangbao@jsut.edu.cn (B.L.); 2024322230@smail.jsut.edu.cn (W.L.)
[2] School of Electrical and Mechanical Engineering, University of Portsmouth, Portsmouth PO1 3DJ, UK
* Correspondence: lei.kang@port.ac.uk

Abstract

Stainless steel is widely used in petrochemical, marine, and electrical engineering applications owing to its excellent corrosion resistance and superior mechanical properties. Electromagnetic acoustic transducers (EMATs), which require no acoustic couplant, are an attractive non-contact ultrasonic technique for the inspection of such materials. However, the amplitude of ultrasonic signals generated and received by EMATs is generally low, which is particularly true for stainless steel test pieces. To overcome this challenge, a novel magnetostrictive-based EMAT incorporating a Terfenol-D coating is proposed in this paper to significantly enhance the ultrasonic signal amplitude. A polymer prepared by mixing Terfenol-D powder with epoxy resin adhesive is applied to the surface of the specimen, serving as an integral part of the EMAT transduction mechanism. Finite element simulation models are established for specimens with and without the Terfenol-D coating using COMSOL Multiphysics 6.0. The distributions of the electromagnetic field and ultrasonic velocity field generated by the proposed EMAT are simulated and analyzed. Experiments are subsequently carried out on the Terfenol-D-coated specimens and the uncoated reference specimens. The effects of the polishing of the coating and the Terfenol-D-to-epoxy weight ratio on the signal enhancement are also experimentally investigated. The results indicate that the proposed EMAT with the Terfenol-D coating can efficiently generate and receive ultrasonic signals. Compared with the conventional EMAT on an uncoated stainless-steel specimen, the received signal amplitude is increased by approximately 6.7×10^3 times. These results suggest that the proposed EMAT is a promising candidate for non-destructive testing and evaluation (NDT&E) applications of stainless-steel specimens.

Keywords: electromagnetic acoustic transducer (EMAT); magnetostrictive-based EMAT; signal amplitude; Terfenol-D coating; non-destructive testing and evaluation (NDT&E)

Check for updates

Academic Editor: Reza K. Amineh

Received: 16 May 2026
Revised: 30 July 2026
Accepted: 31 July 2026
Published: 4 October 2026

Copyright: © 2026 by the authors. Licensee MDPI, Basel, Switzerland. This article is an open access article distributed under the terms and conditions of the Creative Commons Attribution (CC BY) license.

1. Introduction

Austenitic stainless steel, such as SUS 316, is non-ferromagnetic and has been extensively employed in demanding industrial sectors including petrochemicals, offshore and marine structures, and high-voltage electrical equipment, owing to its superior corrosion resistance and excellent mechanical properties. The non-destructive testing and evaluation (NDT&E) of such materials is therefore of great industrial significance. Electromagnetic acoustic transducers (EMATs) are a type of non-contact ultrasonic transducer, capable of generating and detecting ultrasonic waves in electrically conductive and/or ferromagnetic materials [1–4]. A typical EMAT consists of a permanent magnet, a coil, and

a specimen [1,3]. The transduction mechanism of EMATs mainly involves the Lorentz force and the magnetostriction force [5]. In the transmitting process, vibration is produced via electromagnetic coupling and thus generates ultrasonic waves in the test specimen. In the receiving process, the EMAT coil senses the changes in the magnetic and/or electromagnetic fields caused by the surface vibrations of the specimen, thus receiving the ultrasonic signals [1].

However, EMATs generally exhibit relatively low transduction efficiency and thus the amplitude of their generated and received signals is typically weak [6]. This drawback is more pronounced compared to traditional piezoelectric ultrasonic transducers that benefit from direct mechanical coupling. This limitation is especially significant for non-ferromagnetic stainless steel [7]. The amplitude of the received signal measured by an EMAT on non-ferromagnetic stainless steel is approximately 1/4 of that on ferromagnetic stainless steel [4,7]. This makes it challenging to apply EMATs for NDT&E of such industrially important materials.

Research efforts aimed at enhancing the signal amplitude have primarily focused on optimizing the design of the magnet(s) and the coil(s) of the EMATs or on enhancing the input power of the transmitting circuit or the gain of the receiving circuit [1,3,4,6,8–11]. Other research has reported that the signal amplitude of an EMAT depends on the material properties of the specimen [12,13]. A high-performance magnetostrictive strip bonded to the specimen's surface can significantly enhance the signal amplitude of EMATs [12,13]. However, magnetostrictive strips are mainly used for low-frequency guided-wave inspection in the range of tens to hundreds of kilohertz [12,13], and their use for high-frequency bulk-wave or guided-wave inspection at the megahertz level has rarely been reported. An alternative approach is to mix magnetostrictive powder with an adhesive, or to use a physical deposition technique to coat the powder directly onto the specimen [14–21]. Compared with physical deposition, the powder-adhesive mixing approach avoids the inconvenience of transporting and operating the bulky thermal-spray equipment required for on-site industrial inspection. In the authors' previous work, a coating prepared by mixing Fe_3O_4 powder with an adhesive was used to generate and receive bulk waves at 4 MHz, and the signal amplitude was enhanced by approximately 40 times compared with that of a bare steel specimen [15,20]. Nevertheless, there is still considerable room for further improvement.

Among the commonly used magnetostrictive materials, such as pure nickel, iron-cobalt alloy, and iron–gallium alloy, Terfenol-D exhibits significantly superior magnetostrictive properties, due to its large magnetostrictive strain coefficient [22,23]. These characteristics make Terfenol-D promising for enhancing the transduction efficiency of EMATs. However, to the best of the authors' knowledge, a non-conductive polymer coating prepared from Terfenol-D powder and an adhesive has not been reported for high-frequency ultrasonic testing. Therefore, a magnetostrictive-based EMAT with a Terfenol-D coating is studied in this paper to enhance the signal amplitude of high-frequency bulk-wave EMATs for non-ferromagnetic stainless steel, which is difficult to inspect using conventional EMATs.

The organization of this paper is as follows. Section 2 introduces the structure and working principle of the proposed EMAT, along with the key dimensional parameters of its components. Section 3 establishes numerical simulation models for both the conventional EMAT and the new EMAT with Terfenol-D coating, and provides a comparative analysis of the electromagnetic field and ultrasonic wave distributions. Section 4 describes the fabrication of the new EMAT and presents experimental results. Finally, conclusions are drawn in Section 5.

2. Working Principle of the Proposed EMAT

2.1. Structure and Parameters

The schematic diagram of the magnetostrictive-based EMAT with Terfenol-D coating is shown in Figure 1a. The proposed EMAT mainly consists of a coil, a permanent magnet, and a non-ferromagnetic stainless-steel specimen with a Terfenol-D coating on the top surface of the specimen. The permanent magnet is magnetized perpendicular to the surface of the specimen, providing the required static bias magnetic field for EMAT transduction. A copper foil with a thickness of 0.1 mm is attached beneath the magnet as a shielding layer to prevent the generation of spurious ultrasonic waves in the magnet. The EMAT coil is a planar butterfly coil arranged symmetrically, with the input current flowing in the same direction in the linear wires as illustrated in Figure 1b (inside the black solid-line box). A copper foil of the same thickness, serving as a shielding layer, is also attached to the bottom of the non-active sections of the coil, so that only the linear section of the coil is involved in the generation and the reception of ultrasonic waves. It should be noted that the Terfenol-D coating is applied to the surface of the specimen rather than being attached to the EMAT probe; the coating serves as a functional transduction layer on the specimen, while the magnet–coil unit remains fully non-contact with the specimen during inspection.

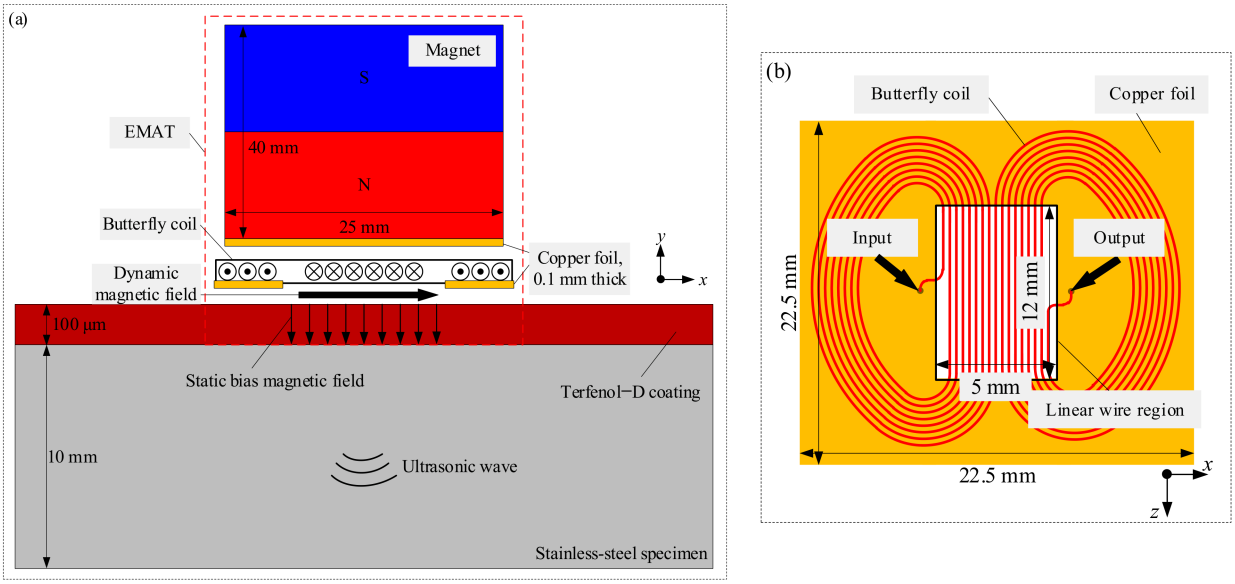

Figure 1. (**a**) Schematic diagram of the magnetostrictive-based EMAT with Terfenol-D coating. (**b**) Schematic diagram of a planar butterfly coil with a copper shielding layer so that only the linear section of the coil is actively involved in the generation and the reception of ultrasonic waves in the stainless-steel specimen. The key dimensions of the permanent magnet, the linear area of the butterfly coil, and the copper shielding foils are annotated in the figure.

The dimensional parameters of the EMAT components are summarized as follows. The permanent magnet measures 35 mm in width, 25 mm in length, and 40 mm in thickness. The non-contact distance between the magnet and the specimen surface is set to 1 mm. The butterfly coil has 34 turns, confined within a 22.5 mm × 22.5 mm area, with the linear wire region in the center measuring 5 mm in width and 12 mm in length. The coil is wound with a copper wire of 0.1 mm in diameter; the lift-off distance between the active area of the coil and the specimen is 0.1 mm. The copper shielding foil beneath the non-active coil sections has a thickness of 0.1 mm. The specimen is made of non-ferromagnetic stainless steel (SUS 316) with dimensions of 50 mm (width) × 50 mm (length) × 10 mm (thickness). The Terfenol-D coating applied to the specimen surface has a thickness of 100 μm, which was selected as a representative value within the range of 50–200 μm.

2.2. Working Principle

An alternating current in the megahertz range is applied to the coil, producing a dynamic alternating electromagnetic field in the coating layer. As the Terfenol-D coating has both electrical conductivity and magnetic properties, the alternating electromagnetic field induces eddy currents and magnetizes the coating. The transduction mechanism of the proposed EMAT includes both Lorentz force and magnetostriction force, each generating ultrasonic waves through a distinct physical pathway.

For the Lorentz force mechanism, the alternating current in the coil induces a corresponding eddy current within the Terfenol-D coating. This eddy current interacts with the external static bias magnetic field provided by the permanent magnet, producing a Lorentz force on the free electrons that acts perpendicular to both the eddy current and the bias field. Through momentum transfer via electron–lattice collisions, ultrasonic waves are generated. The Lorentz force **F** is proportional to the induced eddy current density **J** and the bias magnetic flux density **B** [24]:

$$\mathbf{F} = \mathbf{J} \times \mathbf{B} \tag{1}$$

For the magnetostriction mechanism, the alternating magnetic field generated by the coil current acts on the Terfenol-D coating, causing periodic deformation through the realignment of magnetic domains. This converts electromagnetic energy into acoustic energy, transmitting ultrasonic waves into the test specimen. When the static bias magnetic field is much stronger than the dynamic alternating field, the material responds along a small hysteresis loop around a bias operating point. This magneto-mechanical coupling is governed by the constitutive equation for strain-magnetization [5]:

$$\begin{aligned} \boldsymbol{\varepsilon} &= s_{\mathrm{H}}\boldsymbol{\sigma} + d_{\mathrm{HT}}^{\mathrm{T}}\mathbf{H} \\ \mathbf{B} &= d_{\mathrm{HT}}\boldsymbol{\sigma} + \mu_0\mu_{\mathrm{rT}}\mathbf{H} \end{aligned} \tag{2}$$

where $\boldsymbol{\varepsilon}$ and $\boldsymbol{\sigma}$ are the strain and stress tensors, **B** and **H** are the magnetic flux density and the magnetic field strength, s_{H} and d_{HT} are the elastic compliance matrix and the piezomagnetic coefficient matrix, μ_0 and μ_{rT} are the vacuum permeability and the relative permeability, respectively.

3. Numerical Simulation

3.1. Finite Element Modeling

Finite element models are established using COMSOL Multiphysics. The "Magnetic Fields" module is used to calculate the electric and magnetic fields, while the "Structural Mechanics" module simulates the generation and propagation of ultrasonic waves within the specimen. To efficiently compare the effect of the Terfenol-D coating on the transduction efficiency of the EMATs, only two-dimensional models are employed in the modeling and simulation analysis. The finite element model and its enlarged local view are shown in Figure 2a and Figure 2b, respectively. Simulation models are established for both the conventional EMAT (including an uncoated specimen) and the new EMAT (including a Terfenol-D-coated specimen). For the uncoated specimen, only the Lorentz force coupling method is applied. For the coated specimen, both the Lorentz force and magnetostriction force coupling methods are employed in the coating layer.

The simulation model is a two-dimensional (2D) cross-section in the x–y plane, incorporating four distinct material regions: the permanent magnet, the coil conductors, the Terfenol-D coating layer (100 μm thick, on the top surface of the specimen), and the SUS 316 stainless steel specimen (50 mm wide × 10 mm thick). The coil is modeled as a series of parallel line conductors in the 2D cross-section, each assigned the same current direction.

The inter-wire spacing and conductor diameter are set to 0.05 mm and 0.1 mm, respectively. The surrounding air domain is modeled to capture the far-field magnetic flux distribution. Perfectly matched layer (PML) absorbing boundary conditions are applied at the lateral edges of the specimen (i.e., at both ends of the specimen in the x-direction) to suppress spurious reflections of the simulated ultrasonic waves.

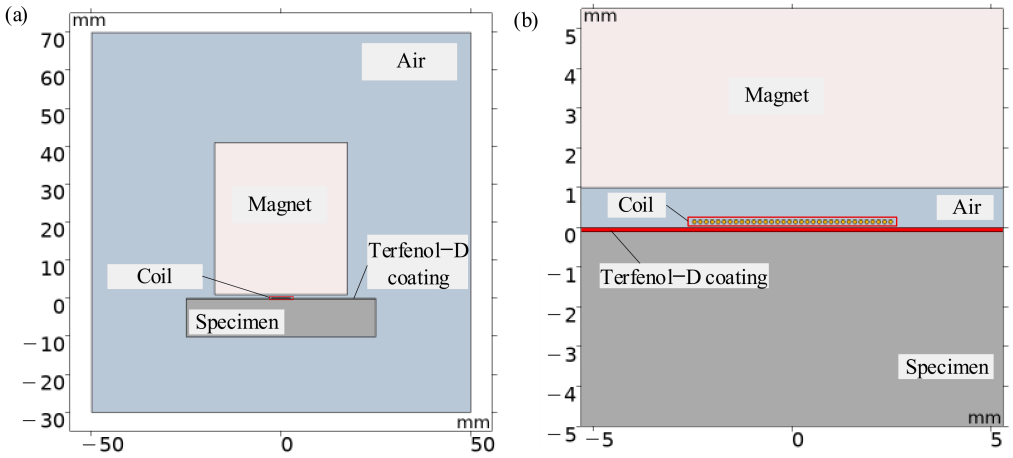

Figure 2. (**a**) Finite element model, and (**b**) enlarged local view of the finite element model.

It should be noted that the main purpose of conducting the simulation analysis In this work is to identify the dominant transduction mechanism of the new transducer and to demonstrate the potential of the signal enhancement of the Terfenol-D coating of the transducer. As the 2D model can efficiently demonstrate the main transduction mechanism and effectively prove the signal enhancement of the new type of transducer, in this study, it is sufficient to conduct the 2D finite element simulation analysis to quickly identify a valid design of the main structure of the new transducer. However, the 2D model neglects the finite aperture of the butterfly coil, the lateral boundaries, and the three-dimensional spreading of the ultrasonic waves. The further optimization of the parameters of the new transducer will need to rely on a more accurate 3D model, which requires more accurate characteristics of the mixture of the Terfenol-D powder and the epoxy, which will be investigated in our future research.

A locally magnified view of the mesh near the Terfenol-D coating layer is shown in Figure 3. The coating region is discretized with a structured quadrilateral mesh with a maximum element size of 40 μm, ensuring at least three elements across the coating thickness. This refined mesh is used to resolve the steep gradients in both the eddy current density and the magnetostriction force within this thin layer. The specimen is also meshed with a structured quadrilateral mesh, with a maximum element size constrained to one-tenth of the shear wavelength (approximately 80 μm at 4 MHz) to guarantee the computation accuracy of the ultrasonic wave propagation [25]. The coil conductors are meshed with a free triangular mesh with a maximum element size of 25 μm. The permanent magnet and the air regions use a coarser meshing strategy to increase computation efficiency without undermining the computation accuracy of the related regions.

The material properties used in the simulation are as follows. For the stainless-steel specimen (SUS 316): electrical conductivity 1.45×10^6 S/m, relative permeability 1.008, density 7.93 g/cm^3, Young's modulus 2.05×10^{11} Pa, and Poisson's ratio 0.285. For the Terfenol-D coating: electrical conductivity 1.67×10^6 S/m, density 9.25 g/cm^3, Young's modulus 2.3×10^{10} Pa, and Poisson's ratio 0.3 [26]. The magnetostrictive properties of the Terfenol-D coating are configured using the strain-magnetization constitutive model

given in Equation (2). The elastic compliance matrix, piezomagnetic coefficient matrix, and permeability parameters of s_H, d_{HT}, and μ_{rT} are set according to reference [22], as follows:

$$s_H = 10^{-11} \cdot \begin{bmatrix} 4.4 & -1.1 & -1.65 & 0 & 0 & 0 \\ -1.1 & 4.4 & -1.65 & 0 & 0 & 0 \\ -1.65 & -1.65 & 3.8 & 0 & 0 & 0 \\ 0 & 0 & 0 & 24 & 0 & 0 \\ 0 & 0 & 0 & 0 & 24 & 0 \\ 0 & 0 & 0 & 0 & 0 & 11 \end{bmatrix} [1/\text{Pa}] \quad (3)$$

$$d_{HT} = 10^{-9} \cdot \begin{bmatrix} 0 & 0 & 0 & 0 & 0 & 16.5 \\ -4.3 & 8.6 & -4.3 & 0 & 0 & 0 \\ 0 & 0 & 0 & 16.5 & 0 & 0 \end{bmatrix} [\text{m/A}] \quad (4)$$

$$\mu_{rT} = \begin{bmatrix} 8.1 & 0 & 0 \\ 0 & 4 & 0 \\ 0 & 0 & 8.1 \end{bmatrix} \quad (5)$$

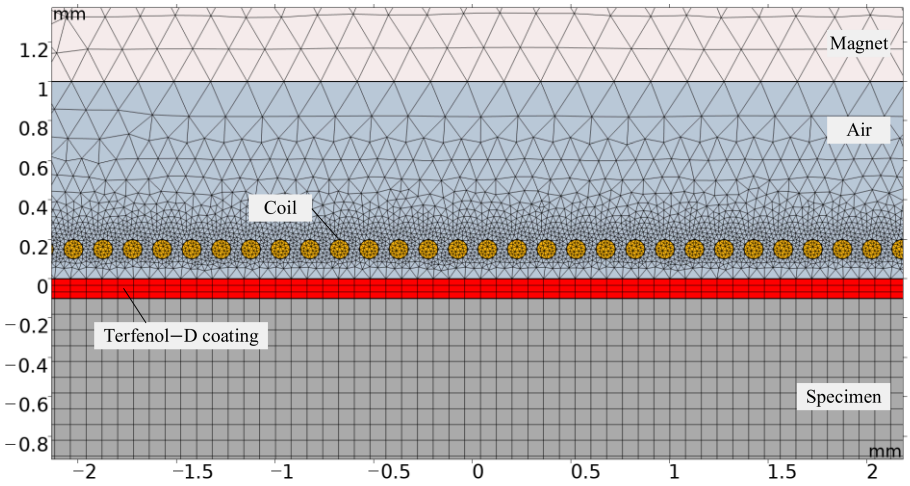

Figure 3. Locally enlarged view of the simulation mesh near the Terfenol-D coating.

3.2. Simulation Analysis

The distribution of the static bias magnetic field generated by the permanent magnet is shown in Figure 4. The magnetic flux density vectors are depicted as arrows overlaid on the color map of the field magnitude. The maximum magnetic flux density is concentrated on the four corners of the magnet, reaching approximately 1.92 T. In the region directly below the linear wire region of the coil, the field is directed perpendicular to the specimen surface, providing the required bias condition for EMAT transduction, with the magnetic flux density at this location reaching approximately 0.5 T, which serves as the static operating point of the new EMAT with the Terfenol-D coating.

The induced eddy current density distributions in the specimen without and with the Terfenol-D coating are shown in Figures 5–7, respectively. For the uncoated specimen (Figure 5), the eddy currents are concentrated within the skin depth of the specimen surface, consistent with a 4 MHz excitation frequency. The electromagnetic skin depth of SUS 316 at 4 MHz is approximately 0.21 mm ($\delta = 1/\sqrt{(\pi f \mu \sigma)} \approx 0.21$ mm, where f is the excitation frequency, μ is the magnetic permeability of the specimen, and σ is the electrical conductivity of the specimen), and the eddy current density decays exponentially with depth into the specimen, as expected from the classical eddy current theory. The peak eddy current density in the uncoated specimen is approximately 1.74×10^8 A/m^2. For the

Terfenol-D-coated specimen with only the electrical conductivity of the coating considered (Figure 6), the relative permeability of the Terfenol-D coating is set to unity (i.e., $\mu_r = 1$) to isolate the pure electrical conductivity effect. Under this condition, the skin depth of the Terfenol-D coating at 4 MHz, given its electrical conductivity of 1.67×10^6 S/m, is approximately 0.19 mm. Since the coating thickness (100 μm) is comparable to this skin depth, the induced eddy currents are predominantly confined within the thin coating layer. Comparing Figure 5 with Figure 6, the peak eddy current density in the coating layer (approximately 2.13×10^8 A/m^2) is elevated relative to that in the uncoated specimen surface. When both electrical and magnetic properties are considered (Figure 7), the eddy current density is further elevated to approximately 5.66×10^8 A/m^2, because the relative permeability of the Terfenol-D coating ($\mu_{rT} \approx 3 \sim 8$) reduces the electromagnetic skin depth ($\delta \propto 1/\sqrt{\mu}$), further concentrating the induced eddy currents within the thin coating layer and thereby elevating the current density.

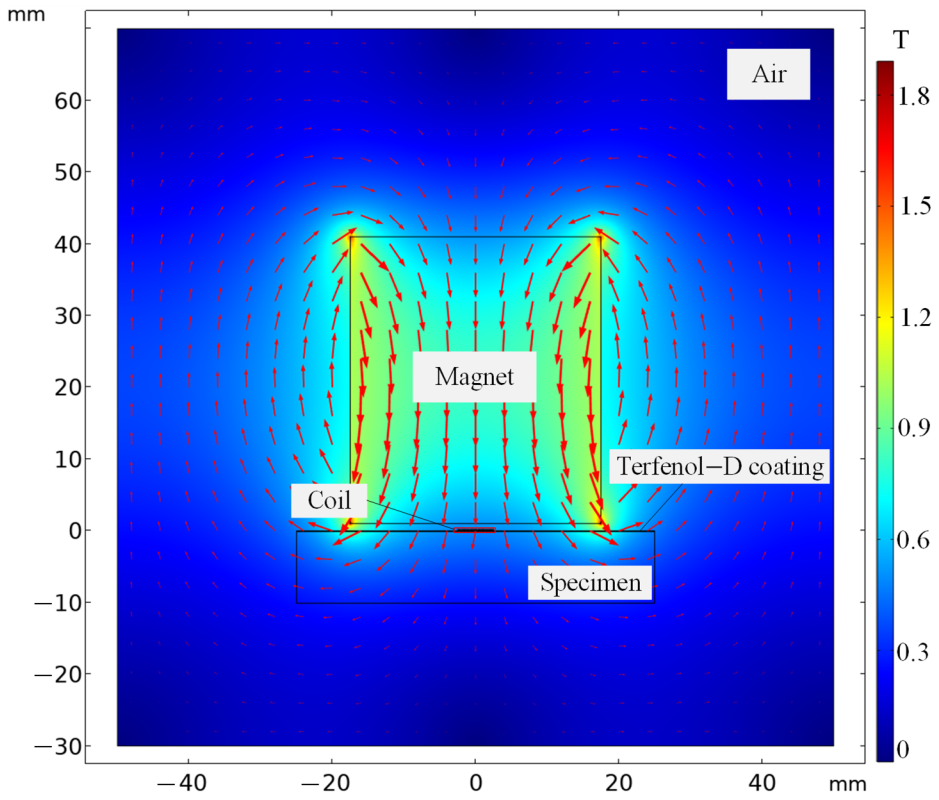

Figure 4. Distribution of the static bias magnetic field generated by the permanent magnet. The color map shows the magnitude of the magnetic flux density in tesla (T), and the arrows represent the magnetic flux density vectors, indicating the direction of the static bias magnetic field.

Theoretically speaking, both the Lorentz force and the magnetostriction mechanisms are involved in the generation and the reception of ultrasonic waves in the new EMAT. To investigate their respective contributions to the generation of ultrasonic waves, the velocity field distributions of the ultrasonic waves are analyzed separately for the two mechanisms.

Figure 8 shows the velocity field distributions obtained from the Lorentz-force-only model for the conventional EMAT. Both shear and longitudinal waves propagate perpendicular to the specimen surface; the longitudinal wave travels at a higher velocity but displays a smaller amplitude. At 0.5 μs, 1.5 μs, and 3 μs, the maximum shear wave amplitudes in the uncoated specimen are 7.36×10^{-4} m/s, 7.14×10^{-4} m/s, and 7.8×10^{-4} m/s, respectively. At 1.5 μs, the amplitude ratio of the shear wave to the longitudinal wave in

the specimen is around 8.7, indicating that this configuration of the conventional EMAT is more suited for generating shear waves.

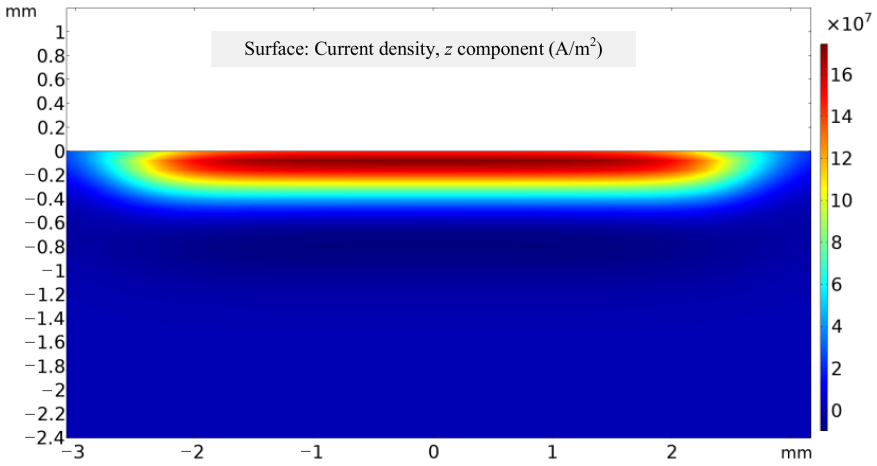

Figure 5. Induced eddy current density distribution in the near-surface layer of the uncoated stainless-steel specimen.

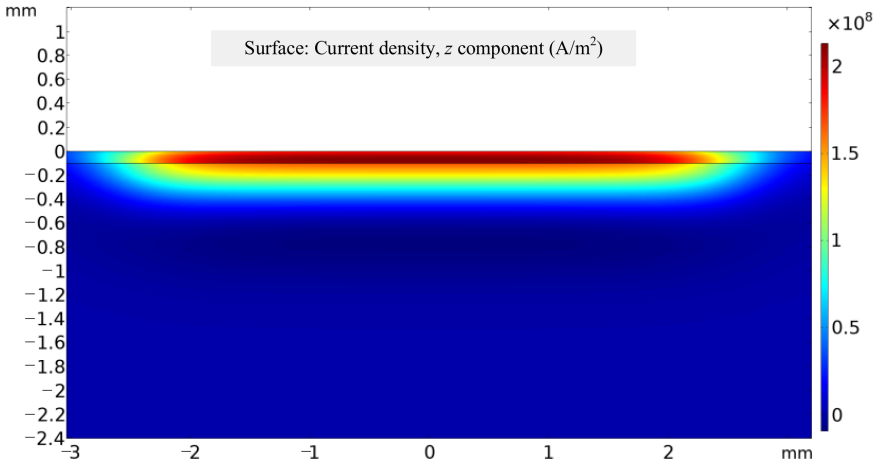

Figure 6. Induced eddy current density in the Terfenol-D-coated specimen (only considering the electrical properties of the coating).

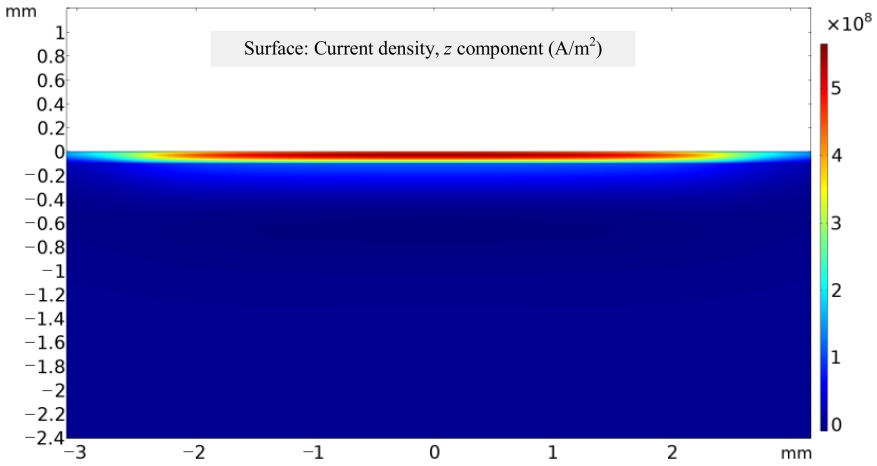

Figure 7. Induced eddy current density in the Terfenol-D-coated specimen (considering both the electrical and the magnetic properties of the coating).

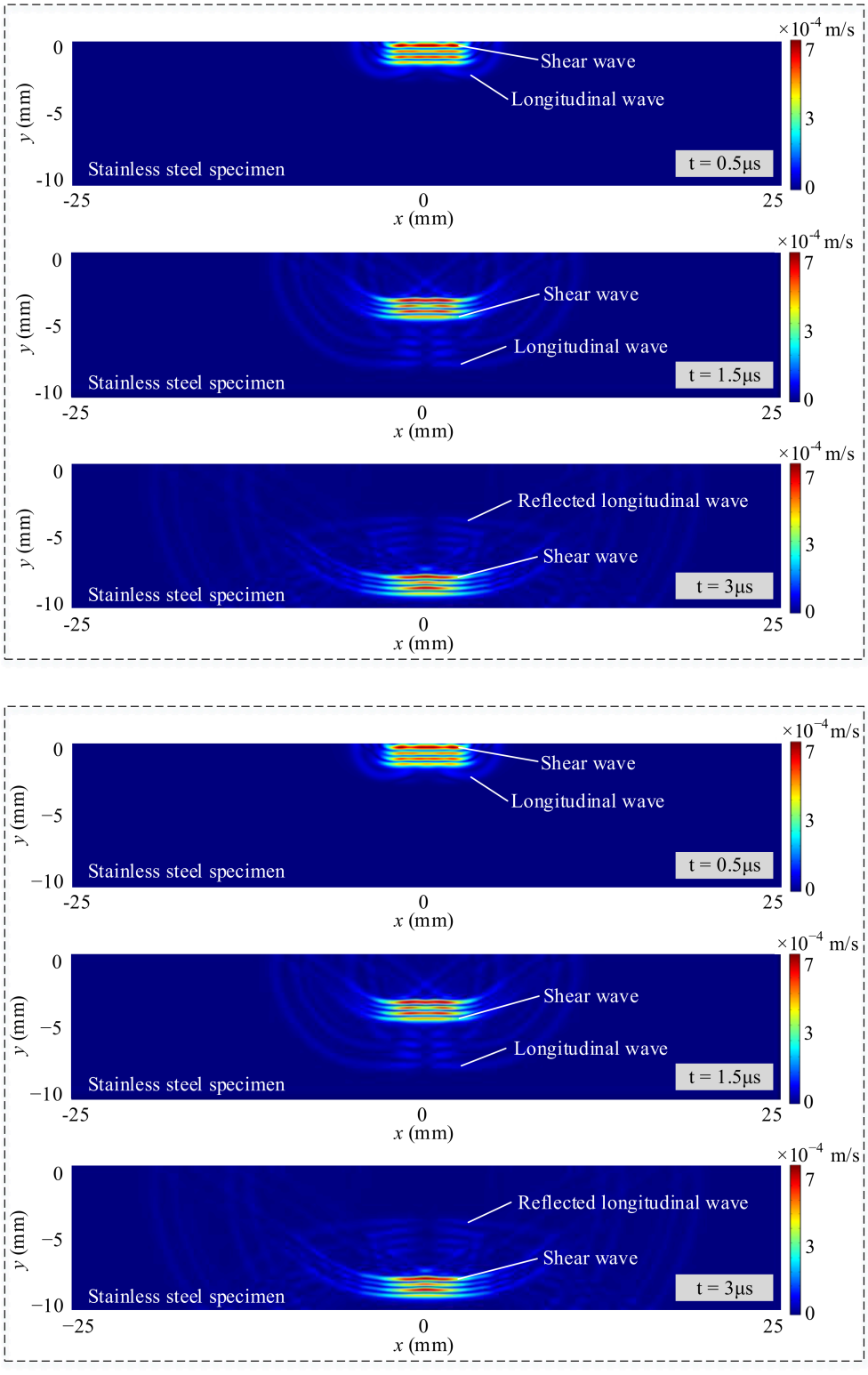

Figure 8. Velocity field distributions of the ultrasonic wave in the specimen without Terfenol-D coating at different times obtained from the Lorentz-force-only model for the conventional EMAT.

Figure 9 shows the velocity field distributions of the ultrasonic wave in the Terfenol-D-coated specimen at different times obtained from the Lorentz-force-only model for the proposed EMAT. At 0.5 μs, 1.5 μs, and 3 μs, the maximum shear wave amplitudes in the Terfenol-D-coated specimen are 1.17×10^{-3} m/s, 3.97×10^{-4} m/s, and 4.56×10^{-4} m/s, respectively. At 1.5 μs and 3 μs, the shear wave amplitudes generated by the Loretz force in the Terfenol-D-coated specimen are approximately 1.80 and 1.71 times lower

than those in the uncoated specimen (Figure 8), respectively. Therefore, when only the Lorentz force contribution is considered, the Terfenol-D coating does not improve the ultrasonic amplitude generated by the EMAT. This reduction may be attributed to the acoustic impedance mismatch at the coating–substrate interface: the Terfenol-D coating reflects the ultrasonic waves, reducing the energy transmitted into the specimen. In addition, a trailing wave component is observable behind the primary shear wave packet at t = 1.5 μs and 3.0 μs. This trailing wave arises from the reflection of the ultrasonic wave within the thin Terfenol-D coating layer.

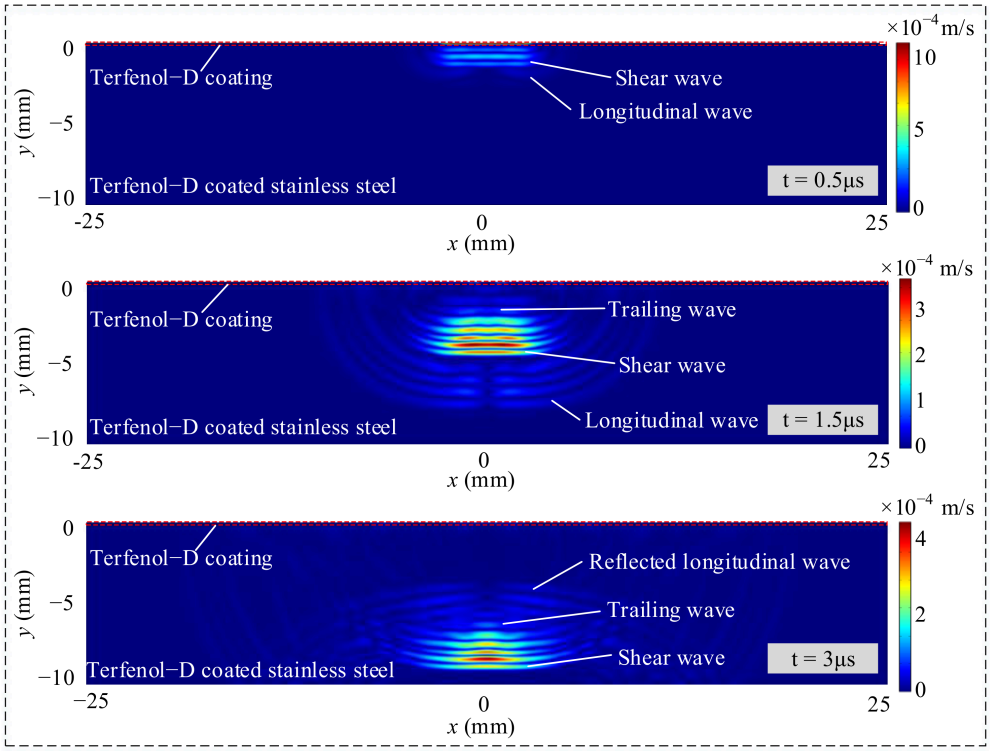

Figure 9. Velocity field distributions of the ultrasonic wave in the specimen with Terfenol-D coating at different times obtained from the Lorentz-force-only model for the proposed EMAT.

Figure 10 shows the velocity field distributions of the ultrasonic wave in the Terfenol-D-coated specimen at different times obtained from the magnetostriction-force-only model for the proposed EMAT. At 0.5 μs, 1.5 μs, and 3 μs, the maximum shear wave amplitudes in the Terfenol-D-coated specimen are 6.31 × 10^{-1} m/s, 4.38 × 10^{-1} m/s, and 4.82 × 10^{-1} m/s, respectively. Comparing these values with those from the Lorentz-force-only model for the uncoated specimen (Figure 8), where the maximum shear wave amplitudes at 0.5 μs, 1.5 μs, and 3 μs are 7.36 × 10^{-4} m/s, 7.14 × 10^{-4} m/s, and 7.8 × 10^{-4} m/s, respectively, the signal amplitude enhancement factors at these three time instants are approximately 8.6 × 10^{2}, 6.1 × 10^{2}, and 6.2 × 10^{2}, respectively.

As demonstrated by the results in Figures 9 and 10, the shear wave amplitude generated by the magnetostriction mechanism is approximately 1.1 × 10^{3} times (e.g., at 1.5 μs and 3 μs) greater than that produced by the Lorentz force alone. The total-field waveform of the proposed EMAT is effectively dominated by the magnetostriction contribution and a separate combined simulation is therefore not presented, as it would offer no additional interpretive value. These results confirm that the Terfenol-D coating substantially enhances the ultrasonic wave amplitude generated by the EMAT, with the magnetostriction mechanism serving as the dominant transduction mechanism. As conventional EMATs primarily operate with the Lorentz force mechanism in non-ferromagnetic stainless steel,

these simulation results also suggest that the signal amplitude of the new EMAT with the Terfenol-D coating can go up to 6.2×10^2 times higher in the generation process than that of a conventional EMAT operating in non-ferromagnetic stainless-steel specimens.

Figures 9 and 10 show that the shear wave amplitude produced by the Lorentz force in the coated specimen is more than two orders of magnitude weaker than that produced by the magnetostriction force; consequently, even if the wave fields generated by the two mechanisms interfered fully constructively or destructively, the total signal amplitude would not change by more than approximately 0.2%. In addition, the non-conductive adhesive chosen for the fabrication of the actual coating layer further reduces the eddy current in the coating layer, and the contribution of the Lorentz force is therefore negligible for the proposed EMAT, and the magnetostriction mechanism can be treated as the dominant transduction mechanism.

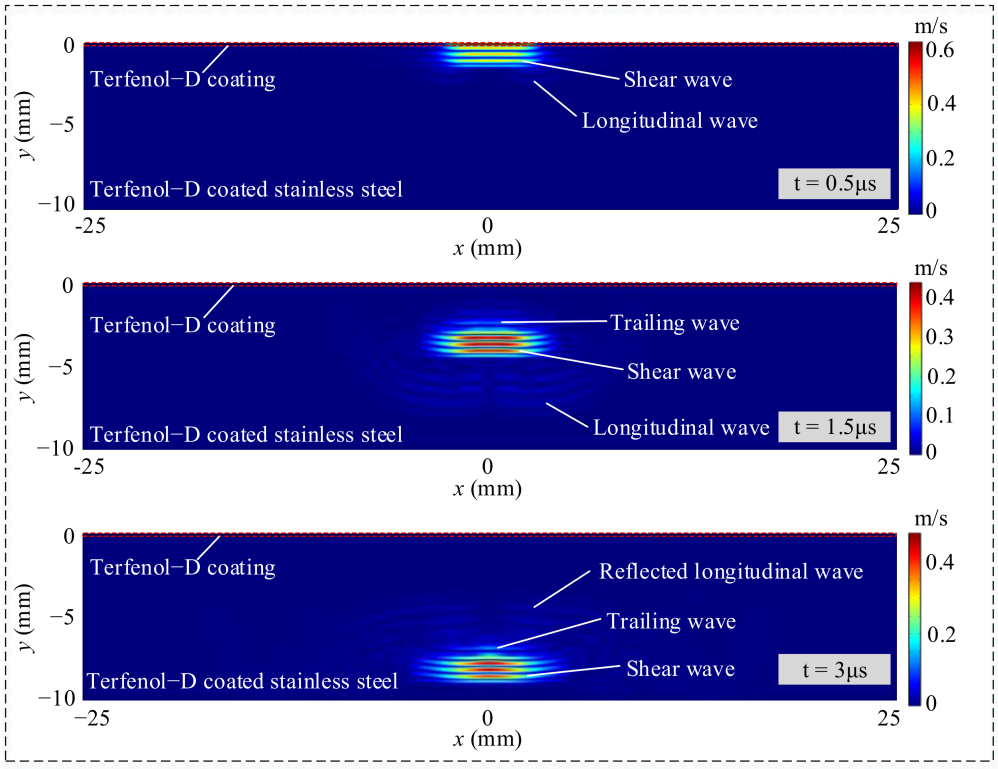

Figure 10. Velocity field distributions of the ultrasonic wave in the specimen with Terfenol-D coating at different times obtained from the magnetostriction-force-only model for the proposed EMAT.

4. Experiments

4.1. Fabrication of the New EMAT

The new EMAT consists of a permanent magnet, a flat butterfly coil, and a non-ferromagnetic stainless steel (SUS 316) specimen with a Terfenol-D coating. The magnet has dimensions of 35 mm in width, 25 mm in length, and 40 mm in thickness, and is magnetized along its thickness direction. A Gauss meter measured a magnetic flux density of approximately 0.5 T at the specimen surface directly beneath the central region of the magnet, at a lift-off distance of approximately 1 mm, following the measurement method described in [15]. The flat butterfly coil has 34 turns and is wound using enameled wire with a diameter of 0.1 mm. The linear wire section in the middle of the butterfly coil is used to generate and receive ultrasonic waves. A 0.1 mm thick copper foil is attached to all non-active areas of the butterfly coil to prevent those regions from generating or receiving ultrasonic signals. An additional copper foil of the same thickness is attached beneath the magnet as a shielding layer.

The specimen is a stainless-steel cylinder with a diameter of 40 mm and a thickness of 10 mm. The Terfenol-D coating is prepared by mixing Terfenol-D powder (average particle size ~10 μm) with a commercial non-conductive epoxy resin adhesive to form a polymer. After curing on the specimen surface, the coating is measured with a calibrated micrometer with an accuracy of 1 μm. The coating is then polished with sandpaper to a thickness of approximately 100 μm. After polishing, the coating thicknesses of three different specimens are measured with the micrometer, and the readings are 97, 100, and 105 μm, indicating that the coating thickness is close to the target value of 100 μm. The use of the electrically insulating epoxy resin as the adhesive serves a dual purpose: it provides sufficient mechanical bonding between the Terfenol-D particles and the specimen to ensure acoustic coupling, while its electrical insulating properties suppress eddy currents, making the magnetostriction-force mechanism even more dominant than the Lorentz-force mechanism.

The magnetostrictive (λ–H) and magnetic hysteresis (B–H) curves of the Terfenol-D material used in this work, provided by the material manufacturer based on experimental measurements, are shown in Figure 11a and Figure 11b, respectively. The λ–H curve shows that the magnetostrictive strain increases rapidly with the applied field at low field strengths and reaches approximately 1568 ppm at a field of 168 kA/m, confirming the strong magnetostrictive behavior of the material. The B–H curve exhibits a typical hysteresis loop, with the magnetization approaching saturation at applied fields of approximately 100 kA/m and a flux density of approximately 0.92 T.

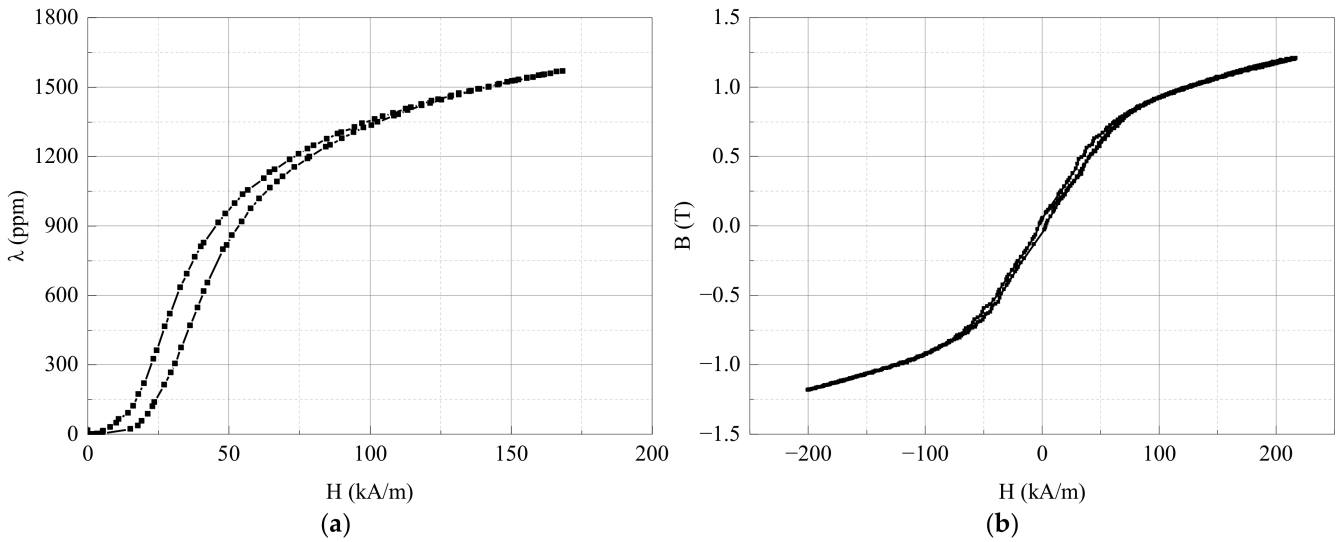

Figure 11. (**a**) Magnetostriction λ–H curve of Terfenol-D, and (**b**) magnetic hysteresis B-H curve of Terfenol-D.

The preparation process of the coating is shown in Figure 12. First, the Terfenol-D powder and the epoxy resin adhesive are weighed to reach a desired weight ratio (Step 1). The powder is then added into the adhesive (Step 2), and they are mixed and stirred until a uniform polymer is obtained (Step 3). After the target surface area of the specimen is cleaned, the polymer is applied onto the surface of the specimen (Step 4), and the coating is cured at room temperature for 24 h (Step 5). After curing, the thickness of the coated specimen is measured with a calibrated micrometer (Step 6). The coating is then polished with different sandpapers, starting with 100-grit and finishing with 400-grit (Step 7), and the thickness is measured again to confirm that the target coating thickness is reached (Step 8). In a practical inspection, this preparation is required only once; the EMAT is then placed above the coated area in a non-contact manner to perform the measurement, whose

potential applications can include periodic ultrasonic inspection and long-term structural health monitoring.

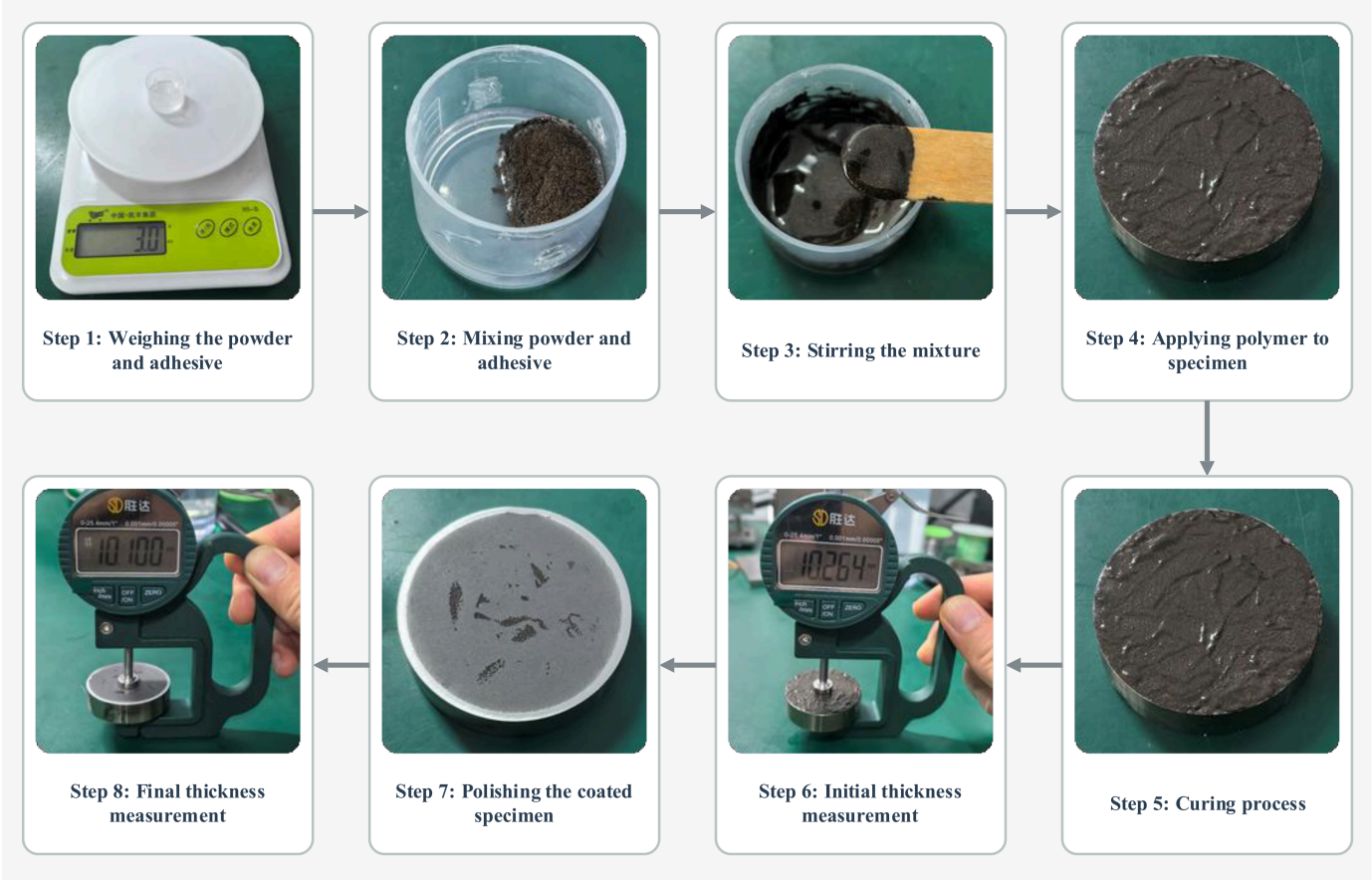

Figure 12. Preparation process of the Terfenol-D coating.

4.2. Experimental Setup

The experimental setup is shown in Figure 13. The setup includes an oscilloscope (KEYSIGHT DSOX2022A), a signal generation and reception circuit, the proposed EMAT, and a test specimen. The circuit incorporates a signal generator, an impedance matching network, and an amplifier–filter circuit. The EMAT coil is excited by a 2-cycle pulse signal with a central frequency of 4 MHz and a peak-to-peak voltage of 1000 V. An impedance matching circuit is used to improve the output power delivered to the EMAT coil. The received signal is amplified with a selectable gain of 20 dB to 80 dB. The amplified signal is then filtered by a bandpass filter with a −3 dB bandwidth of 1 MHz to 5 MHz and displayed on the oscilloscope. The DC power supply, the oscilloscope, the signal generation and reception circuit, and the proposed EMAT are labeled in Figure 13b. The gains of the receiving amplifier used in the experiments are determined by calibration at 4 MHz. A 4 MHz continuous-wave signal with an amplitude of 1 mV is produced by the signal generator and is attenuated to 0.1 mV by a resistive attenuator, so that the input level is comparable to the amplitude of the signals received by the EMATs. The gain of the amplifier is adjusted until the output signal measured on the oscilloscope corresponds to a gain of 20 dB, and then a gain of 60 dB; the two settings are recorded and used in the subsequent experiments. In this way, the gains applied to the received signals of the new and the conventional EMATs have calibrated values of 20 dB and 60 dB, respectively, at 4 MHz.

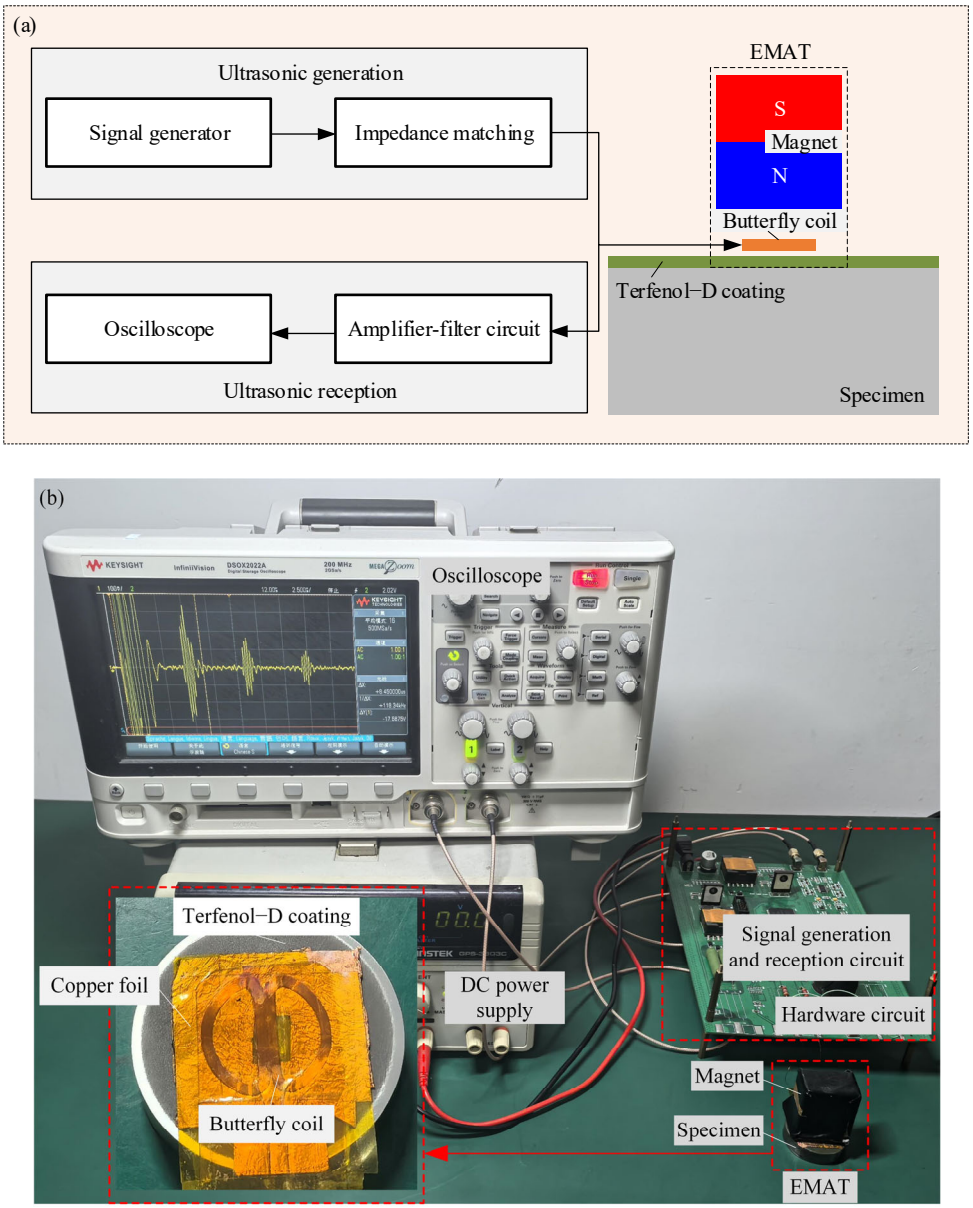

Figure 13. (**a**) Schematic diagram of the experimental setup, and (**b**) photograph of the experimental setup.

4.3. Experimental Results and Discussion

To thoroughly evaluate the performance of the proposed EMAT, two groups of experiments are carried out. The first group is comparative measurements on three uncoated specimens, three coated specimens before polishing, and three coated specimens after polishing; the coatings in this group use a Terfenol-D-to-epoxy weight ratio of 2:1, which is an intermediate value among the weight ratios studied in the second group. The second group is control experiments on the coatings with different Terfenol-D-to-epoxy weight ratios of 1:1, 2:1, and 3:1. In both groups, each test condition is measured on three different specimens to examine the repeatability of the measurements. In all the experiments, the permanent magnet provides a bias magnetic field perpendicular to the specimen surface, with a magnetic flux density of approximately 0.5 T. In the measured waveforms, the "main bang" generated by the excitation pulse and amplified by the receiving circuit does not correspond to an ultrasonic echo signal. Signals labeled S_1, S_2, and S_3 denote the bottom echoes of the first, second, and third shear waves, respectively. In the following analysis, the peak-to-peak values of the first bottom echoes are evaluated.

To ensure a fair comparison between the coated and the uncoated specimens, the bias magnetic field condition, the excitation voltage, the lift-off distances of the coil and the magnet, and the specimen dimensions are all kept identical for the two specimen types. The only difference lies in the gain of the amplifier of the receiving circuit. The maximum output range of the receiving circuit is ±1.25 V. A gain of 60 dB is adopted for the uncoated specimens to make the weak echo signals distinguishable. A much lower gain of 20 dB is adopted for the Terfenol-D-coated specimens to avoid saturation and distortion of the strongly enhanced signals. The gain difference between 60 dB and 20 dB (a factor of 100), which is obtained from the calibration of the receiving amplifier, is compensated for when comparing the signal amplitudes measured under the two gain settings. In addition, all the measurements are carried out with the same receiving circuit and in the same laboratory environment, so that the noise floor referred to the input of the receiving circuit is common to all the measurements. The comparison of the signal amplitudes is therefore made under a common noise floor, and the amplitude enhancement obtained after the gain compensation serves as a direct proxy for the improvement of the signal-to-noise ratio.

(1) Comparative experiments on the uncoated and the coated specimens. Figure 14 shows the representative received signals measured on the uncoated specimen, the coated specimen before polishing (coating thickness of 264 μm), and the coated specimen after polishing (coating thickness of 100 μm). The peak-to-peak values of the first shear-wave bottom echo S_1 measured on all the specimens are summarized in Table 1. The uncoated specimens are measured under a 60 dB gain. The peak-to-peak values of S_1 are 21.7 mV, 22.5 mV, and 25.3 mV, with a mean value of 23.2 mV. Even with such a high receiver gain, distinguishing the echo signals from the noise is relatively difficult. The coated specimens are measured under a 20 dB receiver gain. The unpolished coatings yield S_1 amplitudes of 280.0 mV, 298.2 mV, and 337.0 mV, with a mean value of 305.1 mV. The polished coatings yield 482.4 mV, 519.2 mV, and 519.8 mV, with a mean value of 507.2 mV.

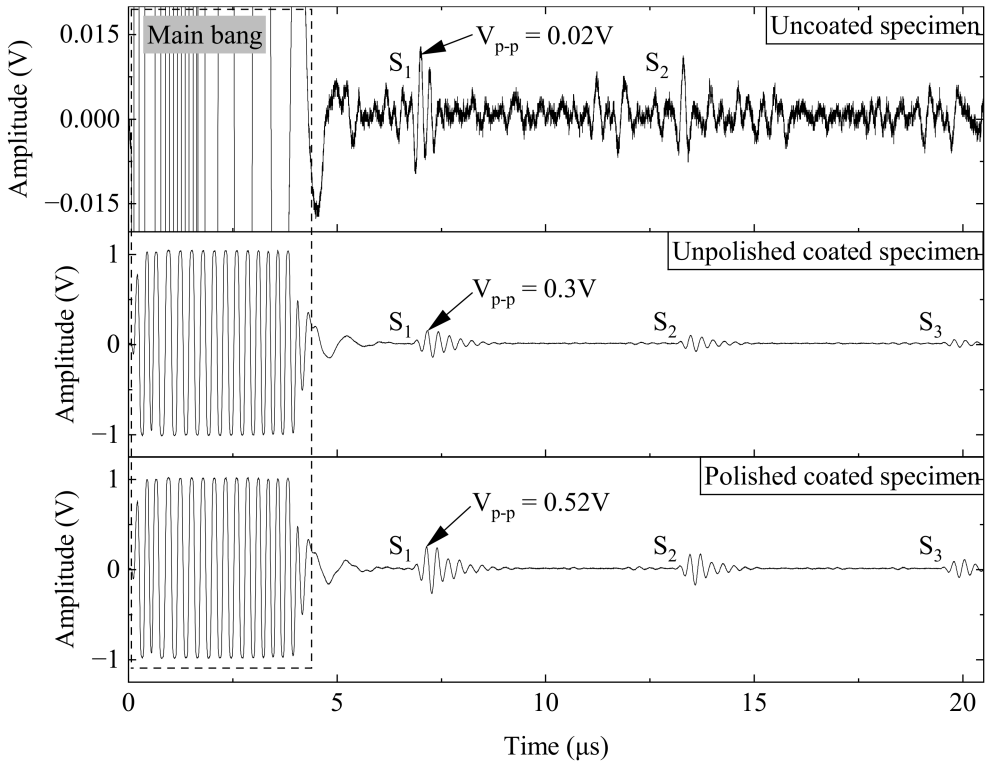

Figure 14. Representative received signals measured on the uncoated specimen (60 dB gain), the coated specimen before polishing (20 dB gain), and the coated specimen after polishing (20 dB gain), under an identical bias magnetic flux density of 0.5 T.

Table 1. Peak-to-peak values of the first bottom echo S_1 measured on the uncoated and the Terfenol-D-coated specimens.

Specimen Condition	Specimen	S_1 Amplitude (mV) [a]	Mean ± SD (mV)	Maximum Deviation
Uncoated	A1 A2 A3	21.7 22.5 25.3	23.2 ± 1.9	±9.2%
Coated, before polishing	A4 A5 A6	280.0 298.2 337.0	305.1 ± 29.1	±10.5%
Coated, after polishing	A7 A8 A9	482.4 519.2 519.8	507.2 ± 21.4	±4.9%

[a] The gains of the receiving amplifiers are 60 dB for the uncoated specimens and 20 dB for the coated specimens.

Two observations can be made from these results. First, after the 40 dB gain difference is compensated for, the mean S_1 amplitude of the polished coated specimens is approximately 2.2×10^3 times that of the uncoated specimens. This result experimentally confirms that the Terfenol-D coating dramatically enhances the transduction efficiency of the EMAT on non-ferromagnetic stainless steel. Second, polishing the coated specimen can increase the signal amplitude. Compared with the unpolished coatings, polishing increases the mean S_1 amplitude by approximately 66%. The maximum deviation of the S_1 amplitude from the mean value also decreases from ±10.5% to ±4.9%. These improvements indicate that a more uniform coating reduces the attenuation within the coating layer and improves the repeatability of the measurements. It may appear counterintuitive that the thinner polished coating yields a higher signal amplitude than the thicker unpolished coating. A likely reason is that the unpolished coating has an uneven and rough surface, which increases the effective lift-off distance and causes stronger scattering and attenuation at the coating surface and within the coating. Polishing makes the coating surface flat and uniform, which reduces this scattering and attenuation. In addition, the thinner coating is very likely more favorable for the constructive interference of the ultrasonic waves that reverberate within the coating, so more acoustic energy is transmitted into the specimen.

(2) Influence of the Terfenol-D-to-epoxy weight ratio on the signal amplitude. Figure 15 shows the representative received signals measured on the specimens coated with Terfenol-D-to-epoxy weight ratios of 1:1, 2:1, and 3:1. All these coatings are polished to the target thickness before the measurements. Three specimens are tested for each ratio, and the results are summarized in Table 2. It should be noted that the vertical scale of the oscilloscope is set to 100 mV, 200 mV, and 500 mV for the weight ratios of 1:1, 2:1, and 3:1, respectively. The scale is chosen according to the signal amplitude to improve the display resolution. The mean peak-to-peak values of S_1 are 169.5 mV, 526.8 mV, and 1553.3 mV for the weight ratios of 1:1, 2:1, and 3:1. That is, the signal amplitude increases monotonically with the Terfenol-D content of the coating within the tested range. The 3:1 coating yields the strongest signal. After the 40 dB gain difference is compensated for, its amplitude is approximately 6.7×10^3 times of the amplitude of the signals received on the uncoated specimens. This behavior is expected, since a higher Terfenol-D content corresponds to a higher Terfenol-D-to-epoxy weight ratio in the polymer coating and hence a stronger overall magnetostrictive response. However, changing the Terfenol-D-to-epoxy weight ratio also changes other properties of the coating, such as its acoustic impedance, elastic modulus, and porosity. The monotonic increase in the signal amplitude with the Terfenol-D

content is therefore consistent with a dominant magnetostrictive contribution, although these accompanying effects may also play a role.

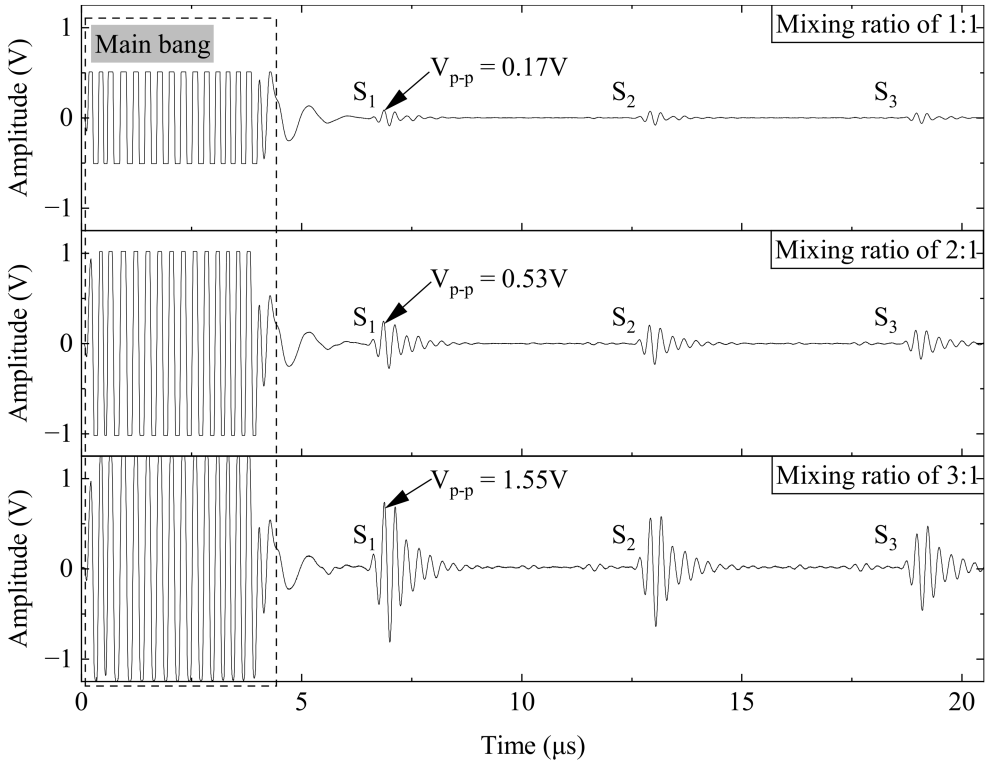

Figure 15. Representative received signals measured on the specimens coated with different Terfenol-D-to-epoxy weight ratios of 1:1, 2:1, and 3:1 (20 dB gain), showing that the signal amplitude increases monotonically with the Terfenol-D content of the coating.

Table 2. Peak-to-peak values of S_1 for the coatings with different Terfenol-D-to-epoxy weight ratios (20 dB gain).

Weight Ratio (Terfenol-D vs. Epoxy)	Specimen	S_1 Amplitude (mV)	Mean ± SD (mV)	Maximum Deviation
1:1	B1	156.3	169.5 ± 11.5	±7.8%
	B2	174.6		
	B3	177.5		
2:1	B4	497.3	526.8 ± 29.9	±5.7%
	B5	526.1		
	B6	557.0		
3:1	B7	1533.1	1553.3 ± 20.9	±1.4%
	B8	1551.9		
	B9	1574.8		

A great enhancement of the signal amplitude of the new EMAT with the Terfenol-D coating has been demonstrated in the experiments. However, it should be noted that the simulated and the measured enhancement factors cannot be compared quantitatively in a one-to-one manner. The simulation only models the generation process of the ultrasonic waves, and the enhancement of 6.2×10^2 times refers to the amplitude of the wave field generated in the specimen. In the actual pulse-echo experiments, both the generation and the reception of the ultrasonic waves benefit from the enhancement effect of the magnetostrictive coating, and thus the measured enhancement of approximately 6.7×10^3 times reflects the combined effect of the two processes, which is why it can exceed the simulated single-process value.

It should also be noted that the geometry of the simulation model differs from that of the experimental specimens. The rectangular cross-section used in the 2D model and the actual cylindrical specimens used in the experiments have the same thickness of 10 mm, but the finite aperture of the coil, the lateral boundaries, and the three-dimensional spreading of the ultrasonic waves are not taken into account in the simulation. The amplitudes predicted by the simulation are therefore only qualitative references rather than quantitative benchmarks for the measured amplitudes.

In addition, the simulation is idealized in several aspects. Firstly, the material parameters used in the simulation (e.g., magnetostrictive coefficient, electrical conductivity, and permeability) correspond to those of bulk Terfenol-D, whereas the experimental coating is a polymer of Terfenol-D powder and epoxy resin, whose physical properties differ from those of the bulk material. Secondly, the simulation assumes the coating consists entirely of Terfenol-D. In the experimental coating, only part of the coating consists of Terfenol-D particles and the rest is epoxy, as set by the Terfenol-D-to-epoxy weight ratio. This gives a lower effective magnetostrictive response than a coating made entirely of Terfenol-D. Thirdly, the simulation assumes a perfectly bonded interface between the coating and the specimen. In practice, the epoxy-bonded interface introduces additional acoustic impedance discontinuities and bonding inefficiencies, which reduce the acoustic energy transmitted from the coating into the substrate. Finally, unlike the rigid solid coating assumed in the simulation, the polymer coating has lower rigidity, which increases acoustic attenuation within the coating layer and further reduces the energy coupled into the specimen. Consequently, the simulated enhancement factor, which accounts for the generation process alone, should be regarded only as a qualitative, upper-bound indicator of the enhancement of the generation efficiency, rather than a quantitative prediction of the absolute amplitude of the signals measured in the experiments.

5. Conclusions

This paper proposes a magnetostrictive-based EMAT incorporating a Terfenol-D polymer coating as a means of enhancing the ultrasonic signal amplitude for NDT&E of non-ferromagnetic stainless steel. The present work focuses on demonstrating the signal amplitude enhancement achievable with this coating approach.

Numerical simulations in COMSOL Multiphysics indicate that magnetostriction is the dominant transduction mechanism of the new EMAT. Experiments on the uncoated and the Terfenol-D-coated specimens show that the received signal amplitude of the new EMAT is increased by approximately 6.7×10^3 times compared with the conventional EMAT. The experiments also show that the signal amplitude increases monotonically with the Terfenol-D-to-epoxy weight ratio within the tested range, and polishing the coating to approximately 100 μm can effectively increase the signal amplitude by approximately 66%.

Future work will focus on the following aspects: the establishment of a refined mathematical model; the validation of defect detectability using specimens containing machined flaws; the optimization of the coating thickness, the powder particle size, and the weight ratio; and the applicability of the proposed approach to curved or geometrically complex specimens and to other material types.

Author Contributions: Conceptualization, B.L. and L.K.; methodology, B.L. and L.K.; software, B.L.; validation, B.L., L.K. and W.L.; formal analysis, B.L.; investigation, B.L. and W.L.; resources, B.L.; data curation, W.L.; writing—original draft preparation, B.L.; writing—review and editing, L.K.; visualization, W.L.; supervision, L.K.; project administration, B.L.; funding acquisition, B.L. All authors have read and agreed to the published version of the manuscript.

Funding: This work is supported by the Basic Science (Natural Science) Research Fund for Higher Education Institutions of Jiangsu Province (No. 25KJB470009), the Industry-University-Research Cooperation Project of Jiangsu Province (No. SG20250075) and the Lateral Research Project of Jiangsu University of Technology (No. KYH25152).

Data Availability Statement: Data will be made available on request.

Conflicts of Interest: The authors declare that they have no known competing financial interests or personal relationships that could have appeared to influence the work reported in this paper.

References

1. Hirao, M.; Ogi, H. *Electromagnetic Acoustic Transducers: Noncontacting Ultrasonic Measurements Using EMATs*; Springer: Tokyo, Japan, 2017.
2. Jian, X.; Dixon, S.; Edwards, R.S.; Morrison, J. Coupling mechanism of an EMAT. *Ultrasonics* **2006**, *44*, 653–656. [CrossRef] [PubMed]
3. Kang, L.; Zhang, C.; Dixon, S.; Zhao, H.; Hill, S.; Liu, M. Enhancement of ultrasonic signal using a new design of Rayleigh-wave electromagnetic acoustic transducer. *NDT E Int.* **2017**, *86*, 36–43. [CrossRef]
4. Zhai, G.; Liang, B.; Li, X.; Ge, Y.; Wang, S. High-temperature EMAT with double-coil configuration generates shear and longitudinal wave modes in paramagnetic steel. *NDT E Int.* **2022**, *125*, 102572. [CrossRef]
5. Ribichini, R.; Cegla, F.; Nagy, P.B.; Cawley, P. Quantitative modeling of the transduction of electromagnetic acoustic transducers operating on ferromagnetic media. *IEEE Trans. Ultrason. Ferroelectr. Freq. Control* **2010**, *57*, 2808–2817. [CrossRef] [PubMed]
6. Pei, C.; Zhao, S.; Xiao, P.; Chen, Z. A modified meander-line-coil EMAT design for signal amplitude enhancement. *Sens. Actuators A Phys.* **2016**, *247*, 539–546. [CrossRef]
7. Ribichini, R.; Cegla, F.; Nagy, P.B.; Cawley, P. Experimental and numerical evaluation of electromagnetic acoustic transducer performance on steel materials. *NDT E Int.* **2012**, *45*, 32–38. [CrossRef]
8. Dixon, S.; Jian, X. Eddy current generation enhancement using ferrite for electromagnetic acoustic transduction. *Appl. Phys. Lett.* **2006**, *89*, 193503. [CrossRef]
9. Ren, W.; He, J.; Dixon, S.; Xu, K. Enhancement of EMAT's efficiency by using silicon steel laminations back-plate. *Sens. Actuators A Phys.* **2018**, *274*, 189–198. [CrossRef]
10. Liu, J.; Liu, S.; Zhang, C.; Jin, L.; Zhao, G. A new focused EMAT design with narrow magnet to achieve both A0-Lamb signal enhancement and waveform distortion correction. *IEEE Sens. J.* **2022**, *22*, 14786–14798. [CrossRef]
11. Rueter, D.; Morgenstern, T. Ultrasound generation with high power and coil only EMAT concepts. *Ultrasonics* **2014**, *54*, 2141–2150. [CrossRef] [PubMed]
12. Kim, Y.Y.; Kwom, Y.E. Review of magnetostrictive patch transducers and applications in ultrasonic nondestructive testing of waveguides. *Ultrasonics* **2015**, *62*, 3–19. [CrossRef] [PubMed]
13. Miao, H.; Li, F. Shear horizontal wave transducers for structural health monitoring and nondestructive testing: A review. *Ultrasonics* **2021**, *114*, 106355. [CrossRef] [PubMed]
14. Qi, Q.; Li, J.; Ding, Z.; Mu, X.; Tang, Z.; Bao, X.; Zhu, J.; Gao, X. Magnetostriction of Fe-Ga coatings and their application in ultrasonic guided wave sensing. *J. Appl. Phys.* **2019**, *125*, 043901. [CrossRef]
15. Liang, B.; Li, Z.; Zhai, G.; Yang, R.; Zhang, X.; Dixon, S. Enhancing the lift-off performance of EMATs by applying an Fe_3O_4 coating to a test specimen. *IEEE Trans. Instrum. Meas.* **2023**, *72*, 9502104. [CrossRef]
16. Glass, S.; Lapeau, J.; Ross, K.; Ali, S.; Hernandez, F.; Lopez, B. Magnetostrictive cold spray sensor for harsh environment and long-term condition monitoring. In Proceedings of the 45th Annual Review of Progress in Quantitative Nondestructive Evaluation, Burlington, VT, USA, 15–19 July 2018; p. 020018.
17. Liang, S.; Ravi, B.G.; Sampath, S.; Gambino, R.J. Atmospheric plasma sprayed cobalt ferrite coatings for magnetostrictive sensor applications. *IEEE Trans. Magn.* **2007**, *43*, 2391–2393. [CrossRef]
18. Lv, F.; Zhang, P.; Tang, Z.; Yue, Y.; Yang, K. A guided wave transducer with sprayed magnetostrictive powder coating for monitoring of aluminum conductor steel-reinforced cables. *Sensors* **2019**, *19*, 1550. [CrossRef] [PubMed]
19. Qi, Q.; Li, J.; Mu, X.; Tang, Z.; Bao, X.; Zhang, P.; Gao, X.; Ding, Z. Microstructure evolution and magnetic properties of annealed magnetostrictive $Fe_{81}Al_{19}$ coatings and their ultrasonic guided wave transducing performance. *Surf. Coat. Technol.* **2019**, *367*, 19–29. [CrossRef]
20. Liang, B.; Li, Z.; Dixon, S.; Yu, Y.; Zhai, G. Development of a magnetostrictive Fe_3O_4-film electromagnetic acoustic transducer. *Sens. Actuators A Phys.* **2023**, *361*, 114593. [CrossRef]
21. Liang, B.; Li, Z.; Tao, W.; Wang, Q.; Yu, Y.; Zhai, G. Giant magneto-acoustic transduction efficiency of a novel magnetostrictive-based electromagnetic acoustic transducer. *Measurement* **2025**, *246*, 116720. [CrossRef]

22. Sherman, C.H.; Butler, J.L. Appendix A.7. In *Transducers and Arrays for Underwater Sound*; Springer: New York, NY, USA, 2007; p. 555.
23. Hathaway, K.B.; Clark, A.E. Magnetostrictive materials. *MRS Bull.* **1993**, *18*, 34–41. [CrossRef]
24. Kawashima, K. Theory and numerical calculation of the acoustic field produced in metal by an electromagnetic ultrasonic transducer. *J. Acoust. Soc. Am.* **1976**, *60*, 1089–1099. [CrossRef]
25. Wang, S.; Kang, L.; Li, Z.; Zhai, G.; Zhang, L. 3-D modeling and analysis of meander-line-coil surface wave EMATs. *Mechatronics* **2012**, *22*, 653–660. [CrossRef]
26. Terfenol-D. Available online: http://tdvib.com/terfenol-d/ (accessed on 20 April 2026).

Disclaimer/Publisher's Note: The statements, opinions and data contained in all publications are solely those of the individual author(s) and contributor(s) and not of MDPI and/or the editor(s). MDPI and/or the editor(s) disclaim responsibility for any injury to people or property resulting from any ideas, methods, instructions or products referred to in the content.